**Few-Body Systems manuscript No.**
(will be inserted by the editor)

# Microscopic description of $^8$Li+nucleus and of $^8$B+nucleus scattering

**P. Descouvemont · E.C. Pinilla**

Received: date / Accepted: date

**Abstract** We apply a microscopic version of the Continuum Discretized Coupled Channel (CDCC) method, referred to as MCDCC, to $^8$Li and $^8$B scattering on different targets. The $^8$Li and $^8$B nuclei are described in a microscopic three-cluster model ($\alpha + t + n$ and $\alpha + {}^3\mathrm{He} + p$), using the hyperspherical coordinates. We first present spectroscopic properties of these nuclei. Then, we determine $^8$Li+nucleus and $^8$B+nucleus potentials by using proton+target and neutron+target interactions. We compute various elastic-scattering cross sections and confirm that breakup effects are important, in particular at low energies. In general, we find a fair agreement with experiment, except for $^8$B+$^{58}$Ni where we suggest that the data might be overestimated.

**Keywords** $^8$Li and $^8$B scattering · CDCC method · Cluster models

## 1 Introduction

Exotic nuclei represent a major interest in current nuclear physics [1]. These nuclei, close to the driplines, are characterized by a low binding energy of the last nucleon(s). This property leads to a halo structure, well known since 30 years [2]. A halo nucleus is considered as a core surrounded by one or two nucleons. Owing to the low binding energy, the spatial extension of the valence nucleons is large, and the associated radii are much larger than in stable nuclei.

Precise reaction theories must include this specific two-body or three-body structure. At energies around the Coulomb barrier, a full quantal treatment of

P. Descouvemont
Physique Nucléaire Théorique et Physique Mathématique, C.P. 229,
Université Libre de Bruxelles (ULB), B 1050 Brussels, Belgium E-mail: pdesc@ulb.ac.be

E.C. Pinilla
Universidad Nacional de Colombia, Sede Bogotá, Facultad de Ciencias, Departamento de Física, Grupo de Física Nuclear, Carrera 45 N° 26-85, Edificio Uriel Gutiérrez, Bogotá D.C. C.P. 1101, Colombia E-mail: ecpinillab@unal.edu.co

the reaction process must be considered. In this energy regime, the Continuum Discretized Coupled Channel (CDCC) method has proved to be an accurate tool [3,4]. The CDCC theory was first developed by Rawitscher [5] to describe deuteron-induced reactions. The low binding energy of the deuteron (2.2 MeV) makes it necessary to include breakup channels, even to determine elastic scattering cross sections.

This traditional CDCC approach, where the projectile is described by a two- or by a three-body structure, faces two major problems: (1) for complex projectiles, such as $^{11}$Li, the three-body model is a rather strong approximation, since it neglects the structure of the core; (2) more important, optical potentials between the target and each constituent of the projectile are often unknown, and crude approximations are sometimes necessary. These problems have been recently addressed by using a microscopic description of the projectile (MCDCC, see Refs. [6–8]). In the MCDCC approach, the projectile wave functions are obtained from a nucleon-nucleon interaction. To describe the scattering process, only nucleon-target optical potentials are necessary. These potentials are well known over a broad range of masses and energies. A first application was performed on the $^7$Li system, where it was shown that the MCDCC provides an excellent description of elastic and inelastic scattering, without any adjustable parameter.

Our aim in the present work is to apply the MCDCC to the $^8$Li and $^8$B three-cluster projectiles. In the spirit of Ref. [6], we use microscopic cluster wave functions, with an exact antisymmetrization between the eight nucleons. We will consider various systems which have been investigated experimentally. The present model offers the possibility of a common study with identical conditions of calculations except, of course, in the nucleon-target interaction.

## 2 Spectroscopy of $^8$Li and $^8$B

### 2.1 Microscopic three-cluster model

The main specificity of the MCDCC [6] is to use a microscopic description of the projectile. In other words, the $^8$Li and $^8$B nuclei are described by a eight-nucleon Hamiltonian, which reads

$$H_0 = \sum_{i=1}^{A_p} t_i + \sum_{i<j=1}^{A_p} (v_{ij}^N + v_{ij}^C), \tag{1}$$

where $A_p = 8$ is the nucleon number, $t_i$ is the kinetic energy of nucleon $i$, $v_{ij}^N$ is an effective nucleon-nucleon interaction, and $v_{ij}^C$ is the Coulomb interaction. Recent few-body calculations [9] use realistic nucleon-nucleon interactions, such as AV18 [10] or CD-Bonn [11]. However we solve the Schrödinger equation associated with (1) within the cluster approximation [12–14]. This approximation permits a precise description of halo states or, more generally, of cluster states where the deformation is large. However, as a consequence,

effective interactions $v_{ij}^N$ must be used, which are adapted to the cluster model. As central force, we adopt the Minnesota interaction [15] which provides a good description of light systems. We also include a zero-range spin-orbit force [16].

Let us write the Schrödinger equation as

$$H_0\,\Phi_{(k)}^{jm\pi} = E_{(k)}^{j\pi}\,\Phi_{(k)}^{jm\pi}, \tag{2}$$

where $j$ and $\pi$ are the angular momentum and parity of the projectile, and where $k$ stands for the excitation level. In the CDCC framework [4,17], the wave functions $\Phi_{(k)}^{jm\pi}$ are expanded over a basis, and the Schrödinger equation (2) is replaced by an eigenvalue problem. Negative energies $E_{(k)}^{j\pi}$ correspond to physical states, whereas positive eigenvalues, referred to as pseudostates (PS), simulate the continuum. Notice that, in some case, a positive eigenvalue may be associated with a physical narrow resonance. If the resonance width is small enough, a bound-state approximation can be used.

In the present work, $\Phi^{jm\pi}$ are defined in a $\alpha+t+n$ (or $\alpha+{}^3\mathrm{He}+p$) three-cluster model, involving $0s$ orbitals for the $\alpha$ and $t$ wave functions $\phi_\alpha$ and $\phi_t$. In the Resonating Group Method (RGM, see Refs. [12,13]), the wave functions are written as

$$\Phi_{(k)}^{jm\pi} = \mathcal{A}\sum_{\gamma}\sum_{K=0}^{\infty}\varphi_{\gamma K}^{jm\pi}(\boldsymbol{\xi}_\alpha,\boldsymbol{\xi}_t,\Omega_\rho)\chi_{\gamma K(k)}^{j\pi}(\rho), \tag{3}$$

where we use the hyperspherical coordinates [18] ($\rho$ is the hyperradius, and $\alpha$ is the hyperangle). In Eq. (3), we define the channel functions as

$$\varphi_{\gamma K}^{jm\pi}(\boldsymbol{\xi}_\alpha,\boldsymbol{\xi}_t,\Omega_\rho) = \phi_\alpha(\boldsymbol{\xi}_\alpha)\left[\left[\phi_t(\boldsymbol{\xi}_t)\otimes\phi_n\right]^S\otimes Y_{\ell_x\ell_y K}^L(\Omega_\rho)\right]^{jm}, \tag{4}$$

where $\boldsymbol{\xi}_\alpha$ and $\boldsymbol{\xi}_t$ are sets of coordinates associated with the $\alpha$ particle, and with the triton, respectively. The total spin $S=0,1$ results from the coupling of the triton and neutron spins, and the total angular momentum $L$ stems from the coupling of $\ell_x$, associated with the $t+n$ coordinate $\boldsymbol{x}$, and $\ell_y$, associated with the $\alpha+(t+n)$ coordinate $\boldsymbol{y}$ (two other choices are possible and are related to each other by unitary transforms). Index $\gamma$ stands for $\gamma=(\ell_x,\ell_y,L,S)$ and the hypermomentum $K$ goes from 0 to infinity (it is limited by $K\leq\ell_x+\ell_y$ and by $(-1)^K=(-1)^{\ell_x+\ell_y}$). In practice it is truncated at a finite value $K_{\max}$. The hypersperical functions $Y_{\ell_x\ell_y K}^{LM}(\Omega_\rho)$ depend on five angles $(\Omega_x,\Omega_y,\alpha)$. We refer the reader to Refs. [16,18] for more detail about the hyperspherical formalism and its application to microscopic three-cluster models.

The unknown quantities in wave functions (3) are the hyperradial functions $\chi_{\gamma K(k)}^{j\pi}(\rho)$. In pratice we use the Generator Coordinate Method (GCM, see Ref. [14]), where these functions are expanded over a set of Gaussian functions centred at different values, called the generator coordinates. In the GCM, the wave function (3) is rewritten as

$$\Phi_{(k)}^{jm\pi} = \sum_{\gamma K}\int dR\, f_{\gamma K(k)}^{j\pi}(R)\,\Psi_{\gamma K}^{jm\pi}(R), \tag{5}$$

where $R$ is the generator coordinate, and $\Psi^{jm\pi}_{\gamma K}(R)$ is a projected Slater determinant. The RGM and the GCM are strictly equivalent, but the GCM definition (5) involves Slater determinants which are well adapted to numerical calculations. The integral in (5) is replaced by a sum over a finite set of generator coordinates (typically $\sim 10$). The Schrödinger equation (2) is therefore converted to an eigenvalue problem, known as the Hill-Wheeler equation,

$$\sum_{\gamma K n}\left[H^{j\pi}_{\gamma K,\gamma' K'}(R_n,R_{n'}) - E^{j\pi}_{(k)}N^{j\pi}_{\gamma K,\gamma' K'}(R_n,R_{n'})\right]f^{j\pi}_{\gamma K(k)}(R_n)=0, \qquad (6)$$

where $H^{j\pi}_{\gamma K,\gamma' K'}(R_n,R_{n'})$ and $N^{j\pi}_{\gamma K,\gamma' K'}(R_n,R_{n'})$ are the Hamiltonian and overlap kernels, respectively. They are obtained from 7-dimension integrals, evaluated numerically [16].

Let us briefly discuss the number of $\gamma K$ values in expansion (3). In Table 1, we present the $\gamma K$ values for $j=2^+$, which corresponds to the $^8$Li/$^8$B ground state. We choose $K_{\max}=4$ which is too small for realistic applications, but large enough for an illustrative example. Even for a small $K_{\max}$, the number of components is rather large (24 here).

**Table 1** Quantum numbers for $j=2^+$ and for $K_{\max}=4$ in expansion (3).

| $S$ | $L$ | $K$ | $\ell_x$ | $\ell_y$ |
|---|---|---|---|---|
| 0,1 | 2 | 2 | 0 | 2 |
| | | | 1 | 1 |
| | | | 2 | 0 |
| | | 4 | 0 | 2 |
| | | | 1 | 1 |
| | | | 1 | 3 |
| | | | 2 | 0 |
| | | | 2 | 2 |
| | | | 3 | 1 |
| 1 | 1 | 2 | 1 | 1 |
| | | 4 | 1 | 1 |
| | | | 2 | 2 |
| 1 | 3 | 4 | 1 | 3 |
| | | | 2 | 2 |
| | | | 3 | 1 |

Table 2 gives the number of $\gamma K$ values, for different $j\pi$, when $K_{\max}$ increases. Clearly these numbers increase very fast with $K_{\max}$. As we will see in the next subsection, typical values are $K_{\max}\sim 16-20$. Compared to $^6$He, the numbers of components are nearly twice as large, since the symmetry of the two neutrons in $^6$He does not exist in $^8$Li and in $^8$B.

When coefficients $f^{j\pi}_{\gamma K(k)}(R_n)$ are determined from (6), various spectroscopic properties can be computed, such as matter, proton and neutron radii, or electromagnetic transition probabilities. To use the GCM wave functions in nucleus-nucleus scattering, the neutron and proton densities of the projectile are required. The calculations must be performed not only for bound

**Table 2** Numbers of $\gamma K$ values for various $j\pi$ and $K_{\max}$.

| $K_{\max}$ | $j = 0^+$ | $j = 1^+$ | $j = 2^+$ | $j = 3^+$ |
|---|---|---|---|---|
| 0 | 1 | 1 | 0 | 0 |
| 4 | 9 | 21 | 24 | 20 |
| 8 | 25 | 65 | 88 | 96 |
| 12 | 49 | 133 | 192 | 228 |
| 16 | 81 | 225 | 336 | 416 |
| 20 | 121 | 341 | 520 | 660 |

states, but also for the pseudostates. The corresponding matrix elements are computed as explained in Ref. [19].

## 2.2 Properties of $^8$Li and of $^8$B

We adopt here an $\alpha + t + n$ microscopic three-cluster model, using the hyperspherical coordinates. This description improves the calculation of Ref. [20], where Jacobi coordinates were used, since the main goal was the investigation of $^7$Li+n and $^7$Be+p scattering and capture. The model spaces were smaller than here since only $\ell_x = 1, 3$ were taken into account (i.e. $j = 1/2^-$ to $7/2^-$, corresponding to the low-lying states of $^7$Li and $^7$Be).

We select eight generator coordinates for the hyperradius ($R$ from 1.5 to 12 fm with a step of 1.5 fm), and $K$ values up to $K_{\max} = 16$. We adopt the Minnesota interaction [15], with a zero-range spin-orbit force. Both terms contain one parameter (admixture parameter $u \approx 1$ in the Minnesota central force, and amplitude $S_0 \approx 30$ MeV.fm$^5$ in the spin-orbit term). Both parameters can be slightly modified to reproduce important properties of the system. We choose $S_0 = 37$ MeV.fm$^5$, which approximately reproduces the energies of the $^7$Li$(1/2^-)$ and $^7$Be$(1/2^-)$ first excited states. For $u$, we take $u = 0.9616$ for $^8$Li and $u = 0.9598$ for $^8$B, which reproduce the binding energies with respect to the $\alpha + t + n$ and $\alpha + {}^3\mathrm{He} + p$ three-body threshold ($-4.49$ MeV and $-1.72$ MeV, respectively). Notice that, with this choice, the binding energies of $^7$Li and $^7$Be are slightly underestimated ($-1.80$ MeV for $^7$Li and $-0.98$ MeV for $^7$Be, to be compared to the experimental values $-2.47$ MeV and $-1.59$ MeV, respectively). We have repeated the calculations by adopting an $u$ value which does reproduce these values, without noticeable change in the cross sections. When the nucleon-nucleon interaction is determined, there is no more free parameter in the model.

In Fig. 1, we present the convergence of $^8$B states with respect to $K_{\max}$. A similar figure is obtained for $^8$Li, and is not shown here. A reasonable convergence is obtained with $K_{\max} \approx 10$, but we use $K_{\max} = 16$ to guaranty a full convergence.

Figure 2 displays energy curves, i.e. energies obtained for a single value of the generator coordinate $R$ in Eq. (6). These energy curves are not used in further calculations, but they provide a useful insight on the properties of the system. Before a full diagonalization of the Hamiltoninan (i.e. by using

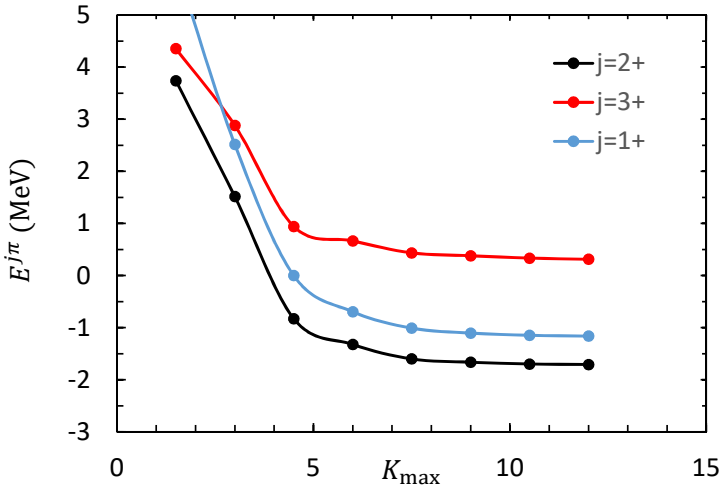


**Fig. 1** Convergence of $^8$B states with respect to $K_{\max}$.

the full set of generator coordinates), we observe a minimum in the $2^+$, $1^+$ and $3^+$ partial waves, were a bound state or a narrow resonance are expected. In agreement with experiment, the lowest minimum is obtained for $j = 2^+$ which corresponds to the ground state of $^8$B. In contrast, negative-parity energy curves are repulsive, which means that no bound states neither narrow resonances can be expected.

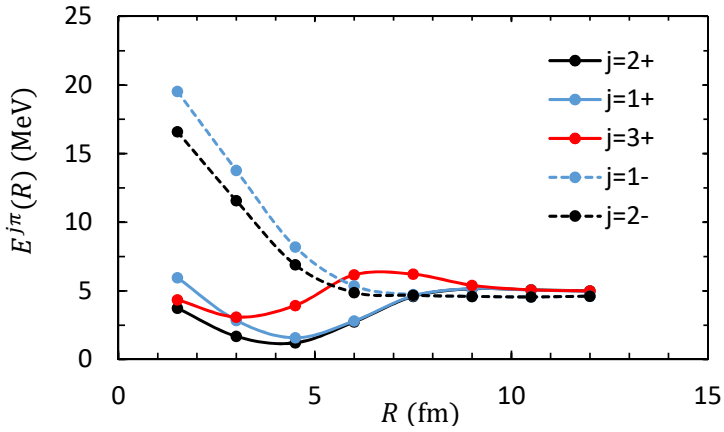


**Fig. 2** $^8$B energy curves, obtained for a single value of the generator coordinate $R$ in Eq. (6).

Table 3 presents various spectroscopic properties of $^8$Li and of $^8$B. The r.m.s. radii are rather well reproduced, as well as the quadrupole moments. In contrast, the $B(E2, 1^+ \to 2^+)$ in $^8$Li, which was measured in 1991 through

Coulomb excitation using a $^8$Li radioactive beam [21,22], is strongly underestimated, as in previous microscopic calculations [23,20,24]. Obviously a remeasurement of the $B(E2)$ would be extremely interesting to clarify the situation. If confirmed, the validity of the model could be questioned.

**Table 3** Spectroscopic properties of $^8$Li and $^8$B.

| | $^8$Li | | | $^8$B | | |
|---|---|---|---|---|---|---|
| | GCM | exp | Ref. | GCM | exp | Ref. |
| $\sqrt{< r^2 >}$ (fm) | 2.35 | $2.37 \pm 0.02$ | [25] | 2.45 | $2.38 \pm 0.04$ | [25] |
| $\sqrt{< r^2 >_p}$ (fm) | 2.16 | $2.26 \pm 0.02$ | [25] | 2.58 | $2.45 \pm 0.05$ | [25] |
| $\sqrt{< r^2 >_n}$ (fm) | 2.46 | $2.44 \pm 0.02$ | [25] | 2.21 | $2.28 \pm 0.04$ | [25] |
| $Q(2^+)$ ($e$.fm$^2$) | 2.3 | $3.27 \pm 0.06$ | [26] | 5.3 | $6.83 \pm 0.21$ | [26] |
| $B(E2)$ (W.u.) | 1.6 | $47 \pm 23, 87 \pm 23$ | [21,22] | 5.0 | | |
| $E(1^+)$ (MeV) | 0.69 | 0.98 | [26] | 0.55 | 0.77 | [26] |
| $E(3^+)$ (MeV) | 1.88 | 2.26 | [26] | 1.98 | 2.32 | [26] |

The neutron and proton monopole densities of the ground states are shown in Fig. 3. We define the normalization as in Ref. [27]. As expected, the neutron density of $^8$Li, and the proton density of $^8$B extend to large distances. These densities, as well as those of the pseudostates (see next section) will be used to compute the $^8$Li/$^8$B+nucleus potentials and the corresponding cross sections.

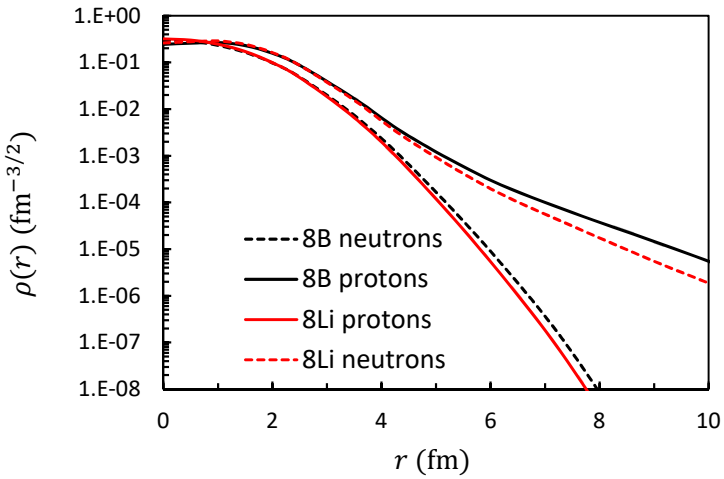


**Fig. 3** Neutron and proton densities of the $^8$Li and of $^8$B ground states.

## 3 Microscopic model for $^8$Li and $^8$B scattering

### 3.1 Overview of the MCDCC

The microscopic CDCC (see Refs. [6,7]) is a natural extension of the traditional CDCC method [4,17], where the breakup of the projectile is simulated by pseudostates. The Hamiltonian of the projectile + target system is defined as

$$H = H_0 + T_R + \sum_{i=1}^{A_p} v_{iT}(\boldsymbol{r}_i - \boldsymbol{R}), \tag{7}$$

where $H_0$ is the Hamiltonian of the projectile, $\boldsymbol{R}$ is the projectile-target relative coordinate, and $\boldsymbol{r}_i$ are the internal coordinates of the projectile. The interaction between nucleon $i$ and the target $T$ reads

$$v_{iT}(\boldsymbol{s}) = \big(\frac{1}{2} - t_{iz}\big)\left[v_{pT}(\boldsymbol{s}) + \frac{Z_T e^2}{s}\right] + \big(\frac{1}{2} + t_{iz}\big) v_{nT}(\boldsymbol{s}), \tag{8}$$

where $\boldsymbol{t}_i$ is the isospin of nucleon $i$, $Z_T e$ is the charge of the target, and $v_{pT}(\boldsymbol{s})$ and $v_{nT}(\boldsymbol{s})$ are proton and neutron optical potentials, respectively.

The total wave function, associated with Hamiltonian (7) is expanded over the GCM basis (2) as

$$\Psi^{JM\pi} = \frac{1}{R}\sum_{cL} \mathcal{Y}_{cL}^{JM\pi}(\Omega_R)\, u_{cL}^{J\pi}(R), \tag{9}$$

where $L$ is the relative angular momentum, and index $c$ stands for the projectile states $c = (j,k)$. We assume that the target has a spin $0^+$ and remains in its ground state. The channel functions are given by

$$\mathcal{Y}_{cL}^{JM\pi}(\Omega_R) = i^L \big[\Phi^j_{(k)} \otimes Y_L(\Omega_R)\big]^{JM}, \tag{10}$$

where $\Phi^j_{(k)}$ are the internal wave functions (3) (the parity is implied). In expansion (9), the summation over the pseudostates is limited by truncations on angular momentum $j_{\max}$, and on excitation energy $E_{\max}$. The radial functions $u_{cL}^{J\pi}(R)$ are solutions of the coupled-channel system

$$-\frac{\hbar^2}{2\mu}\left[\frac{d^2}{dR^2} - \frac{L(L+1)}{R^2}\right] u_{cL}^{J\pi}(R) + \sum_{c'L'} V_{cL,c'L'}^{J\pi}(R) u_{c'L'}^{J\pi}(R) = (E - E_c) u_{cL}^{J\pi}(R), \tag{11}$$

where $E_c$ are the projectile energies given by Eq. 2, and where the coupling potentials $V_{cL,c'L'}^{J\pi}(R)$ are obtained from the matrix elements

$$V_{cL,c'L'}^{J\pi}(R) = \langle \mathcal{Y}_{cL}^{JM\pi} | \sum_{i=1}^{A_p} v_{iT}(\boldsymbol{r}_i - \boldsymbol{R}) | \mathcal{Y}_{c'L'}^{JM\pi} \rangle. \tag{12}$$

These matrix elements are calculated from the densities of the projectile (see Ref. [28] for details). The coupled-channel system (11) is solved with the $R$-matrix method, using Lagrange meshes [29,30]. This method provides the radial functions $u_{cL}^{J\pi}(R)$ and the corresponding scattering matrices. Cross sections are then computed with standard formulas.

### 3.2 Application to $^8$Li-nucleus scattering

The conditions of the GCM description of $^8$Li have been given in Sect.2.2. Figure 4 shows the pseudostates included in the calculation (energies are given with respect to the $\alpha + t + n$ threshold). Only three states can be considered as physical: the $2^+$ ground state, the $1^+$ first excited state, and the low-energy $3^+$ resonance. As presented in Table 3, the GCM properties are in fair agreement with experiment.

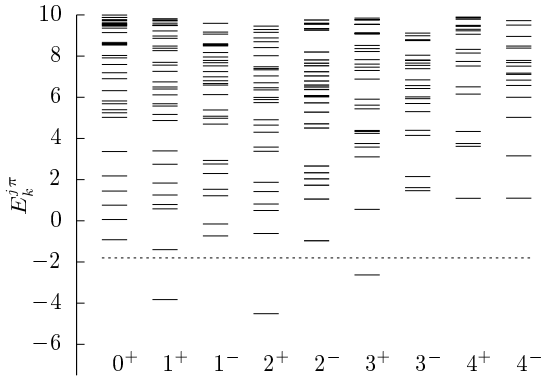


**Fig. 4** Bound and pseudostates energies $E_k^{j\pi}$ of $^8$Li as a function of its total angular momentum $j^\pi$. The $^8$Li energies are defined from the $\alpha + t + n$ breakup threshold. The dashed line indicates the $^7$Li+n two-body threshold.

For the nucleon-target interaction $v_{iT}$, we use the global parametrization of Koning and Delaroche [31]. The $R$-matrix channel radius is taken as $a = 30$ fm with $N = 120$ mesh points. These conditions guaranty that the nuclear interaction is negligible in the external region ($R \geq a$), and that the internal wave function can be described with accuracy. Various tests have been performed to check that the cross sections are insensitive to these parameters.

One of the important issues in CDCC calculations is the convergence with respect to the number of pseudostates. This is controlled by two parameters, $j_{\max}$ and $E_{\max}$. The convergence of the MCDCC has been illustrated previously for other reactions (see, for example, refs. [27,32]). The situation is similar here, and we only present the single-channel and the full calculations. This comparison illustrates the role of breakup effects.

In Fig. 5, we present elastic cross sections for $^8$Li+$^{12}$C at $E_{\rm lab} = 14$ MeV ($E_{\rm c.m.} = 8.4$ MeV), and for $^8$Li+$^{209}$Bi at $E_{\rm lab} = 37$ MeV ($E_{\rm c.m.} = 35.6$

MeV). Experimental data are taken from Ref. [33] and Ref. [34], respectively. For $^{8}$Li+$^{12}$C, the experimental angular distribution contains very few angles, and does not provide evidence for an oscillatory behaviour. Breakup effects are stronger at large angles ($\theta > 50°$, where nuclear effects are important), and improves the agreement with the available data. Scattering to an heavy target is illustrated with $^{8}$Li+$^{209}$Bi, with the recent data of Ref. [34]. Without breakup, the model overestimates the data around $\theta \approx 50°$, and predicts too small cross sections at large angles. Although there is a slight underestimation at $\theta > 60°$, breakup effects improve the agreement with experiment. Most likely, transfer channels such as $^{209}$Bi($^{8}$Li,$^{7}$Li)$^{210}$Bi are not negligible, although they are not included in CDCC calculations.

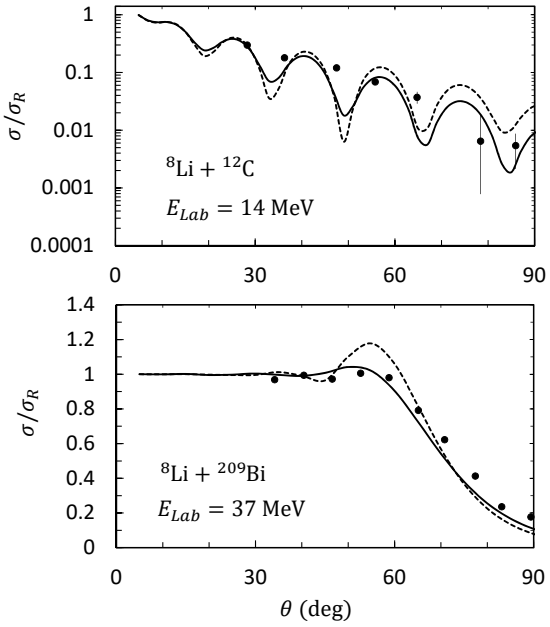


**Fig. 5** $^{8}$Li+$^{12}$C (upper panel) and $^{8}$Li+$^{209}$Bi (lower panel) elastic cross sections (divided by the Rutherford cross sections). The data are taken from Ref. [33] and Ref. [34]. The dotted line represents the single-channel calculation, and the solid line corresponds to the full calculation.

### 3.3 Application to $^{8}$B-nucleus scattering

The conditions are identical to those of $^{8}$Li+nucleus scattering. Figure 6 illustrates the model with $^{8}$B+$^{12}$C and $^{8}$B+$^{208}$Pb, and the experimental data are taken from Refs. [35] and [36], respectively. As for $^{8}$Li, the data on $^{8}$B+$^{12}$C are

too few to show a possible oscillatory structure, as predicted by the theory. Further experiment would be welcome. At high energies, the application to $^{8}$B+$^{208}$Pb shows that breakup effects are weak.

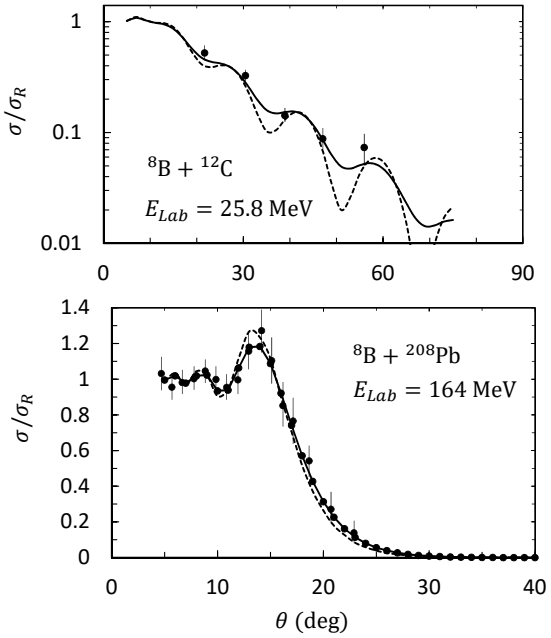


**Fig. 6** $^{8}$B+$^{12}$C (upper panel) and $^{8}$B+$^{208}$Pb (lower panel) elastic cross sections (divided by the Rutherford cross sections). The data are taken from Ref. [35] and Ref. [36]. The dotted line represents the single-channel calculation, and the solid line corresponds to the full calculation.

We want to address more specifically the data on $^{8}$B+$^{58}$Ni [37], which are presented in Fig. 7. As shown in this figure, the agreement with the data is poor, even when breakup effects are included. A similar disagreement is obtained at other energies. Although there might be specific effects on $^{8}$B+$^{58}$Ni, it is surprising to see that other theoretical approaches face some problems in the analysis of the data. In Ref. [37], the authors provide optical potentials which do fit the data, but the real part of the potential is unphysically small compared to the imaginary part. In Ref. [38], the authors use microscopic densities of the $^{8}$B ground state to investigate elastic scattering on different targets. As usual, the folding potential is renormalized to simulate the missing breakup effects. This factor is quite different from unity for densities obtained in a three-body model (between 0.4 and 0.2, depending on energy). Although the fits presented in Ref. [38] nicely agree with experiment, the associated pa-

rameters are open to criticism. These results suggest that the data on $^8$B+$^{58}$Ni could be too large, and should be reconsidered.

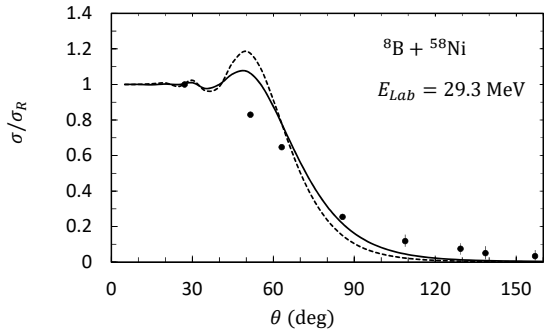


**Fig. 7** $^8$B+$^{58}$Ni elastic cross section (divided by the Rutherford cross sections). The data are taken from Ref. [37]. The dotted line represents the single-channel calculation, and the solid line corresponds to the full calculation.

## 4 Conclusion

In this paper, we have applied the MCDCC to elastic scattering involving $^8$Li and $^8$B as projectile. These nuclei are described by 8-body wave functions, defined in the framework of the RGM/GCM. This model provides a fair description of spectroscopic properties, except for the $B(E2)$ in $^8$Li, whose experimental value is larger by one order of magnitude. This disagreement confirms previous theoretical works [23,20,24]. A re-measurement of this transition probability would be very helpful to clarify the situation.

The elastic cross sections have been determined in a coupled-channel formalism, where the potentials are deduced from the projectile wave functions. As usual in CDCC calculations, pseudostates represent an approximation of the three-body continuum, and simulate breakup effects. As the nucleon-target optical potentials are taken from the literature, there is no fitting parameter in the model. We have investigated elastic scattering on a light target, with $^8$Li+$^{12}$C and $^8$B+$^{12}$C. For heavy targets, we have considered three systems: $^8$Li+$^{209}$Bi, $^8$B+$^{208}$Pb and $^8$B+$^{58}$Ni. There is a reasonable agreement for the first two reactions, but the MCDCC cannot reproduce satisfactorily the data on $^8$B+$^{58}$Ni. We have mentioned that the problem is also present, although not explicitly pointed out, in other theoretical approaches.

The CDCC method is a powerful tool to study reactions involving weakly bound nuclei. Using pseudostates allows a realistic treatment of breakup effects, known to be important for the scattering of exotic nuclei. The method

involves large coupled-channel systems, and is demanding in terms of computer times. The calculation of scattering matrices is performed by using the $R$-matrix theory which is fast and accurate.

Of course, the CDCC method only includes elastic and breakup channels. Rearrangement channels, in particular nucleon transfer to the target, could be a role, even in the elastic cross section. Including transfer channels in the CDCC theory represents a challenge for future scattering calculations [39].

**Acknowledgements** This work was supported by the Fonds de la Recherche Scientifique - FNRS under Grant Number 4.45.10.08. It benefited from computational resources made available on the Tier-1 supercomputer of the Fédération Wallonie-Bruxelles, infrastructure funded by the Walloon Region under the grant agreement No. 1117545.

## References

1. I. Tanihata, H. Savajols, R. Kanungo, Prog. Part. Nucl. Phys. **68**, 215 (2013)
2. I. Tanihata, H. Hamagaki, O. Hashimoto, Y. Shida, N. Yoshikawa, K. Sugimoto, O. Yamakawa, T. Kobayashi, N. Takahashi, Phys. Rev. Lett. **55**, 2676 (1985)
3. M. Kamimura, M. Yahiro, Y. Iseri, S. Sakuragi, H. Kameyama, M. Kawai, Prog. Theor. Phys. Suppl. **89**, 1 (1986)
4. N. Austern, Y. Iseri, M. Kamimura, M. Kawai, G. Rawitscher, M. Yahiro, Phys. Rep. **154**, 125 (1987)
5. C. Rolfs, R.E. Azuma, Nucl. Phys. A **227**, 291 (1974)
6. P. Descouvemont, M.S. Hussein, Phys. Rev. Lett. **111**, 082701 (2013)
7. P. Descouvemont, E.C. Pinilla, M.S. Hussein, Few-Body Systems **56**, 737 (2015).
8. P. Descouvemont, N. Itagaki, Phys. Rev. C **97**, 014612 (2018).
9. B.R. Barrett, P. Navrátil, J.P. Vary, Prog. Part. Nucl. Phys. **69**, 131 (2013).
10. R.B. Wiringa, V.G.J. Stoks, R. Schiavilla, Phys. Rev. C **51**, 38 (1995).
11. R. Machleidt, F. Sammarruca, Y. Song, Phys. Rev. C **53**, R1483 (1996)
12. H. Horiuchi, Prog. Theor. Phys. Suppl. **62**, 90 (1977)
13. K. Wildermuth, Y.C. Tang, *A Unified Theory of the Nucleus* (Vieweg, Braunschweig, 1977)
14. P. Descouvemont, M. Dufour, *Clusters in Nuclei*, vol. 2 (Springer, 2012)
15. D.R. Thompson, M. LeMere, Y.C. Tang, Nucl. Phys. A **286**, 53 (1977)
16. S. Korennov, P. Descouvemont, Nucl. Phys. A **740**, 249 (2004)
17. M. Yahiro, K. Ogata, T. Matsumoto, K. Minomo, Prog. Theor. Exp. Phys. p. 01A206 (2012)
18. M.V. Zhukov, B.V. Danilin, D.V. Fedorov, J.M. Bang, I.J. Thompson, J.S. Vaagen, Phys. Rep. **231**, 151 (1993)
19. D. Baye, P. Descouvemont, N.K. Timofeyuk, Nucl. Phys. A **577**, 624 (1994)
20. P. Descouvemont, D. Baye, Nucl. Phys. A **573**, 28 (1994)
21. R.J. Smith, J.J. Kolata, K. Lamkin, A. Morsad, F.D.B. andJ. A. Brown, W.Z. Liu, J.W. Jänecke, D.A. Roberts, R.E. Warner, Phys. Rev. C **43**, 2346 (1991)
22. J.A. Brown, F.D. Becchetti, J.W. Jänecke, K. Ashktorab, D.A. Roberts, J.J. Kolata, R.J. Smith, K. Lamkin, R.E. Warner, Phys. Rev. Lett. **66**, 2452 (1991)
23. P. Descouvemont, D. Baye, Phys. Lett. B **292**, 235 (1992)
24. P. Descouvemont, Phys. Rev. C **70**, 065802 (2004)
25. I. Tanihata, T. Kobayashi, O. Yamakawa, S. Shimoura, K. Ekuni, K. Sugimoto, N. Takahashi, T. Shimoda, H. Sato, Phys. Lett. B **206**, 592 (1988)
26. D.R. Tilley, J.H. Kelley, J.L. Godwin, D.J. Millener, J.E. Purcell, C.G. Sheu, H.R. Weller, Nucl. Phys. A **745**, 155 (2004)
27. P. Descouvemont, Phys. Rev. C **93**, 034616 (2016).
28. J. Grineviciute, P. Descouvemont, Phys. Rev. C **90**, 034616 (2014).
29. P. Descouvemont, D. Baye, Rep. Prog. Phys. **73**, 036301 (2010)

30. P. Descouvemont, Comput. Phys. Commun. **200**, 199 (2016).
31. A.J. Koning, J.P. Delaroche, Nucl. Phys. A **713**, 231 (2003)
32. P. Descouvemont, T. Druet, L.F. Canto, M.S. Hussein, Phys. Rev. C **91**, 024606 (2015).
33. A. Barioni, V. Guimarães, A. Lépine-Szily, R. Lichtenthäler, D.R. Mendes, E. Crema, K.C.C. Pires, M.C. Morais, V. Morcelle, P.N. de Faria, R.P. Condori, A.M. Moro, D.S. Monteiro, J.M.B. Shorto, J. Lubian, M. Assunção, Phys. Rev. C **80**, 034617 (2009).
34. K.J. Cook, I.P. Carter, E.C. Simpson, M. Dasgupta, D.J. Hinde, L.T. Bezzina, S. Kalkal, C. Sengupta, C. Simenel, B.M.A. Swinton-Bland, K. Vo-Phuoc, E. Williams, Phys. Rev. C **97**, 021601 (2018).
35. A. Barioni, J.C. Zamora, V. Guimarães, B. Paes, J. Lubian, E.F. Aguilera, J.J. Kolata, A.L. Roberts, F.D. Becchetti, A. Villano, M. Ojaruega, H. Jiang, Phys. Rev. C **84**, 014603 (2011)
36. Y.Y. Yang *et al.*, Phys. Rev. C **87**, 044613 (2013)
37. E.F. Aguilera, E. Martinez-Quiroz, D. Lizcano, A. Gómez-Camacho, J.J. Kolata, L.O. Lamm, V. Guimarães, R. Lichtenthäler, O. Camargo, F.D. Becchetti, H. Jiang, P.A. DeYoung, P.J. Mears, T.L. Belyaeva, Phys. Rev. C **79**, 021601 (2009)
38. V.K. Lukyanov, D.N. Kadrev, E.V. Zemlyanaya, K.V. Lukyanov, A.N. Antonov, M.K. Gaidarov, K. Spasova, Eur. Phys. J. A **53**(2), 31 (2017).
39. S.R. Cotanch, C.M. Vincent, Phys. Rev. C **14**, 1739 (1976).